Cortical consequences of comorbidity: distinct effects of hearing loss and the 22q11.2 deletion on temporal processing in the auditory cortex

Chen Lu[1], Jennifer F. Linden[1,2*]

1 Ear Institute, University College London, London, WC1X 8EE, UK

2 Department of Neuroscience, Physiology, & Pharmacology, University College London, London WC1E 6BT, UK

Abstract

Peripheral hearing loss can cause auditory hallucinations and is considered a risk factor for psychosis, at least in genetically vulnerable individuals. To disentangle brain abnormalities driven by hearing loss and genetic risk for psychosis, we quantified auditory cortical temporal acuity in mice with or without hearing loss and with or without a genetic risk factor for psychosis (22q11.2 deletion). We recorded cortical activity while awake mice listened to loudness-adjusted gap-in-noise stimuli with varying durations of silent gap. Both hearing loss and the 22q11.2 deletion were associated with impairments in auditory cortical temporal acuity. However, hearing loss broadly impaired temporal acuity of neural population activity, while the 22q11.2 deletion had more subtle effects, selectively impairing gap duration thresholds in regular-spiking (putative excitatory) but not fast-spiking (putative inhibitory) neurons. Results suggest that auditory cortical consequences of comorbid hearing loss and genetic risk for psychosis are at least partially dissociable.

Keywords

Gap detection threshold, auditory cortex, *Df1*/+ mouse, Neuropixels, temporal processing, 22q11.2 Deletion Syndrome

Introduction

Clinical studies have shown that psychosis impairs auditory processing, including frequency discrimination, spatial localization, deviant detection, and prepulse inhibition [1]. In addition, patients with psychosis exhibit reduced hearing sensitivity and difficulty hearing in noisy environments [2,3]. Although hearing loss is recognized as a risk factor for psychosis [4], it remains unclear whether it merely co-occurs with other psychosis risk factors or independently exacerbates the risk or severity of the disorder.

Temporal processing is essential for normal auditory function, supporting sound perception and speech recognition [5–7]. It can be quantified using the gap-in-noise paradigm, which measures sensitivity to brief silent gaps embedded within white noise or pure tones. Patients with psychosis exhibit prolonged gap detection thresholds, indicating impaired auditory temporal acuity [8,9]. In the general population, peripheral hearing loss also increases gap detection thresholds, even when sound levels are adjusted to compensate for elevated hearing thresholds [10]. Here, we investigated how hearing loss and genetic risk for psychosis interact to influence auditory cortical activity evoked by gap-in-noise stimuli, aiming to disentangle their respective contributions to auditory dysfunction.

We used *Df1/+* mice, a model of 22q11.2 deletion syndrome (22q11.2DS), to study how hearing loss and genetic risk shape auditory cortical temporal processing. The 22q11.2 deletion is one of the most common chromosomal microdeletions, with a prevalence of 1 in every 2,200 live births [11]. Nearly 25% of carriers develop schizophrenia in their lifetime — compared to 0.5% in the general population — and their symptoms are similar to idiopathic schizophrenia [12]. The deletion also confers a high incidence of conductive hearing loss, with over half of carriers experiencing early-onset middle-ear inflammation [13]. *Df1/+* mice, which harbor a homologous chromosomal deletion, exhibit similar comorbid hearing loss in approximately 50% of animals and show electrophysiological brain abnormalities paralleling those observed in human deletion carriers [14,15].

In this study, we investigated how genetic and experiential risk factors for psychosis interact to influence auditory function by comparing *Df1/+* mice with normal hearing or hearing loss to wild-type (WT) mice with normal hearing or hearing loss (2x2 experimental design). We asked how auditory cortical sensitivity to brief gaps differed between animal groups with well-controlled genetic background and well-characterised hearing sensitivities. Intracranial recordings from auditory cortical neurons were obtained using Neuropixels probes while awake mice listened passively to gap-in-noise stimuli with sound levels adjusted to compensate for the hearing threshold of each mouse. Novel, robust methods for quantifying gap-duration thresholds at both the single-neuron and neuronal population levels provided rigorous metrics of auditory cortical temporal acuity in each animal group. These methods revealed that both peripheral hearing loss and the 22q11.2 deletion disrupt auditory cortical temporal acuity, however, the effects of these two risk factors differ across cortical cell types. Together, our findings demonstrate a new experimental approach to disentangling the effects of multiple risk factors for psychosis, and provide a foundation for translational studies of the impact of comorbid hearing loss on psychosis pathology in humans.

Methods

Animals

Df1/+ mice were originally developed from a 129SvEvBrd X C57BL/6J background [16] and had been maintained on a C57BL/6J background for well over 25 generations, through pairing of *Df1/+* males either with WT females from the colony or (at least yearly) with newly acquired C57BL/6J females from Charles River UK. WT mice used in this study were also C57BL/6J mice purchased from Charles River UK. Mice were raised in standard cages and mouse housing facilities, on a standard 12 h-light/12 h-dark cycle. All experiments were performed in accordance with a Home Office project licence approved under the United Kingdom Animal Scientific Procedures Act of 1986.

Malleus removal surgery

Approximately half of *Df1/+* mice experience chronic hearing impairment in one or both ears, arising from early-onset middle ear inflammation which causes conductive hearing loss [14,17]. To generate an early-onset and comparable conductive hearing loss in a subset of WT animals, we performed malleus removal in WT mouse pups at P11, before the opening of the ear canal [18,19]. Pups were anaesthetised with isoflurane (3% for induction, 1.5-2% for maintenance with 2 L/min O_2) and body temperature was maintained at 37 °C using a homeostatic heat pad. Carprofen (5 mg/kg body weight) was administered subcutaneously for analgesia. A postauricular skin incision was made and the cartilage forming the ear canal was cut through to expose the tympanic membrane. After piercing the tympanic membrane, the malleus was removed by grasping the orbicular apophysis through this opening using a pair of fine forceps. The skin was then closed with Vetbond Tissue Adhesive (3M). Once recovered from anaesthesia in a warm cage (30-35 °C), the pups were returned to the nest together with their siblings. For sham surgeries, every step was performed identically except that the tympanic membrane was left intact and the malleus was not removed.

Auditory brainstem response recording

The setup for auditory brainstem response recording was the same as described previously [15].

Intracranial recording with Neuropixels 1.0 probe

Acoustic stimuli

Auditory stimuli were generated using customised software written in MATLAB. Stimuli were converted to an analog signal using an external sound interface (RME Fireface UC), amplified via an amplifier (ROTEL), and played through a speaker (Peerless by Tymphany). The speaker was positioned 10 cm in front of the animal. The speaker output was calibrated to within ± 0.2 dB of the maximal calibration values (100 dB SPL for 8–64 kHz tones, 105 dB SPL for 16 kHz tone) using a free-field 1/4" microphone (G.R.A.S.), positioned at the location of the mouse's head.

The frequency-response area (FRA) stimulus was composed of pure tones ranging from 8 to 64 kHz, with 8 steps per octave. The sound intensity was adjusted based on the better-ear hearing threshold of the mouse ranging from -20 to 30 dB HL in 5 dB increments relative to the hearing threshold. When

the hearing thresholds differed between ears, the threshold of the better-hearing ear was used to avoid overstimulation. Each tone was played for 50 ms, with 5-ms onset and offset ramps, and the inter-stimulus interval was 500 ms. Different tones were presented in a pseudo-random order with 3 repetitions.

The noise level for the gap-in-noise stimulus was also adjusted for each mouse, to be 20 dB above the better-ear hearing threshold. The gap-in-noise stimulus was composed of a pair of white noise bursts, with a gap duration in the middle varying from 0 to 256 ms (0, 1, 2, 4, 8, 16, 32, 64, 128, 256 ms). The white noise was synthesized by summing discrete pre-calibrated pure tones from 8 to 64 kHz, spaced at 8 steps per octave. The first noise burst lasted for 250 ms, followed by a gap, and the second noise burst lasted for 100 ms. To avoid blurring the broadband transients, no ramping was used. The inter-trial interval was 1000 ms, and each gap had 45 repetitions. All trials were pseudo-randomized.

Animal procedures

Adult mice were anaesthetized with isoflurane (3% for inducting and 1.25-1.75% for maintaining with 2 L/min O_2). An incision was made along the midline to expose the skull. The craniotomy site was marked for acute recording (AP -2.2 to -3.6 mm, ML 2.5 to 3.2 mm from Bregma). A small hole was drilled above the left frontal lobe, and a bone screw connected to a male pin was inserted for grounding. The bone screw and the headpost were fixed onto the skull using dental adhesive resin cement (Super-bond, Sun Medical). A well was constructed around the pre-marked craniotomy site. Dental cement was used to reinforce the walls of the well and to protect the wire and the base of the pin. The well was sealed with silicone sealant (Kwik-Cast, WPI) to protect the exposed skull. Warm saline (0.1 mL) was administered subcutaneously for hydration before removing the mouse from anaesthesia. Carprofen (0.02–0.025 mg/mL in drinking water) was provided for the first three days following surgery.

Mice were habituated gradually to increasing durations of head-fixation for at least 5 days before the acute recording day to reduce stress.

On the morning of the acute recording, a craniotomy was performed following the marked site to expose the brain tissue. Anaesthesia was induced and briefly maintained with isoflurane (3% for induction and 1.25–2% for maintenance with 2 L/min O_2). Carprofen (5 mg/kg body weight) and dexamethasone (0.2 mg/kg body weight) were administered subcutaneously. A craniotomy well was drilled along the marked trace to expose the brain tissue. Saline and silicone sealant (Kwik-Cast, WPI) were used to protect the exposed brain tissue. Warm saline was administered for hydration before the mouse was removed from anaesthesia.

Once the mouse had recovered from anaesthesia, it was head-fixed in the recording apparatus. The silicone sealant cap was removed, and the craniotomy site was filled with sterile saline. A Neuropixels 1.0 probe (IMEC) stained with fluorescent dye DiO (Invitrogen) was gradually inserted into the brain tissue. The probe was referenced to the implanted bone screw and grounded to the anti-vibration table. Neural signals were transmitted to the headstage (IMEC), then to the PXIe acquisition module (IMEC) installed in a PXI chassis (PXIe-1071, National Instruments) and finally to the host computer.

The probe was gradually lowered to a depth of 2000–2500 μm at an extremely slow speed of 2–2.5 μm/s with a micromanipulator (Sensapex). The recording software SpikeGLX was opened to monitor the changes in the signal when lowering the probe. After 10-minute settling for the probe, the recording was then started. Once the recording was complete, the probe was retracted at a speed of 5 μm/s for the first 100 μm, and then at a speed of 50μm/s for the remaining distance. The craniotomy site was washed with sterile saline and covered with silicone sealant before returning the mouse to the cage in the warm incubator.

Typically, each mouse underwent two recording sessions on the day when the craniotomy was opened. The interval between two recording sessions was usually around 3 hours, during which time the mouse was returned to a standard cage in a quiet, warm environment. The probe was cleaned using 1% Tergazyme enzyme detergent in lukewarm double-distilled water (~30 °C) and then rinsed and soaked in double-distilled water for re-use.

After recordings were completed, mice were euthanized using pentobarbital (0.2 – 0.3 mL of 20 mg/mL). Following transcardiac perfusion with phosphate-buffered saline and subsequently with 4% paraformaldehyde, the brain tissue was harvested and soaked in 4% paraformaldehyde for an additional 24 hours. The brain tissue was sectioned into 50 μm slices using a vibratome (Leica VT1200S). Sections were mounted with DAPI Fluoromount-G (Invitrogen) and imaged using a widefield microscope (Zeiss Axio Imager 2).

Data processing

Preprocessing

Preprocessing was performed using the SpikeInterface [20]. Action potential recordings were initially corrected for phase shifts and band-pass filtered (300–9000 Hz). Bad channels, which included damaged recording sites or sites located outside of the brain, were identified and removed. The signals were then re-referenced using a global common median reference to eliminate common noise. Spiking events were extracted from the signals using Kilosort 2.5 [21]. A quality matrix was calculated to exclude invalid units based on the waveform features of units: amplitude median was set above 50 μV, amplitude cutoff was set below 0.25, inter-spike interval violation was set below 0.2, and isolation distance was above 15.

Putative fast-spiking units and regular-spiking units were clustered based on the peak-trough intervals and peak-trough ratios [22,23]. Units classified as positive (with peak amplitude higher than trough amplitude) were excluded from further analysis [24]. A Gaussian mixture model was applied and only units with clustering probabilities greater than 0.95 were retained.

Likely primary auditory units were defined based on physiological features: significant, short-latency tone-evoked responses. Frequency response area trials involving all tones presented at intensity levels above the animal's hearing threshold were pooled, and firing rates were compared between the 50-ms periods before and after tone onset to identify units with significant tone-evoked responses (Wilcoxon test, $p<0.01$). Then, the same pooled trials were then used to construct a post-stimulus time histogram (PSTH) with 2-ms bins, to identify the earliest bin following sound onset in which firing rate

exceeded 3 standard deviations around the mean spontaneous firing rate in the 50-ms period before sound onset. If this latency was less than 50 ms, then the tone-responsive unit was defined as a likely primary (core) auditory cortical unit.

Data analysis

Animals were grouped based on their genotypes and hearing sensitivities in both ears, as measured with click-evoked ABR at week 8 (*Df1*/+ HL: *Df1*/+ mice with both ears having hearing loss; *Df1*/+ NH: *Df1*/+ mice with both ears normal hearing; WT HL: WT mice with malleus removal surgery in both ears; WT NH: WT mice with sham surgery in both ears). Since sound levels for all stimuli were adjusted to be constant relative to the better-ear hearing threshold for each mouse, and since neural recordings were made in the right auditory cortex (which is most strongly driven by the left ear), we focused our analysis on animals for which the left ear was the better-hearing ear.

Statistical tests are defined in the text when used and were conducted two-tailed with $\alpha=0.05$ unless noted otherwise. Analysis of onset and offset responses, single-unit gap-duration thresholds, and population-level gap-duration thresholds are described briefly below and more extensively in the Results section.

Onset and offset response detection

The onset and offset responses of single units were detected by comparing neural responses before and after transient events in noise. Significant changes in firing rates were defined as 2 consecutive rising bins within the post-transient event period that exceeded 3 standard deviations above the mean of the pre-transient event period. For sound onset responses, we also allowed for the possibility of drops in firing rate due to sound-evoked inhibition; however, we required offset responses to manifest as an increase in firing rate because a decrease in firing rate following sound offset cannot easily be distinguished from recovery from adaptation in the absence of sound-evoked activity [25]. The pre-onset period is the 100 ms before the first noise onset, and the post-onset period is 100 ms after the first noise onset. The pre-offset period is 50 ms before the second noise offset, and the post-offset period is 10 to 110 ms after the second noise offset. Onset and offset analyses were performed for all trials. A unit was classified as onset- or offset-responsive only if at least 7 out of the 10 gap conditions exhibited valid responses as defined above.

Identification of gap duration thresholds in single units

Gap detection in single units was analyzed by comparing deviations in neural responses surrounding gaps to sustained responses to noise. The peri-gap analysis window spanned from the start of the gap to 100 ms after the gap ended, covering the entire gap and second noise period. The sustained response to noise was measured as the neural response during the last 100 ms of noise in the trial with a 0-ms gap. The root mean squared deviation (RMSD) of neural responses within the peri-gap analysis window, relative to the sustained responses, was calculated as below:

$$RMSD = \sqrt{\frac{1}{T}\sum_{t=1}^{T} (x_t - \mu_0)^2}$$

where x_t is spike rate of 5-ms bin at time t, μ_0 is the mean firing rate in the last 100 ms of noise in the no-gap condition, and T is the total number of time bins within the peri-gap analysis window.

A sigmoid function was fitted to quantify the relationship between the normalized RMSD and the binary logarithm of gap duration (in ms). In some cases, RMSD values decreased at longer gap durations or were close to zero for shorter gaps, which could reduce the quality of the sigmoid fit. In such instances, the fitting was performed again after excluding these problematic data points. The better-fitting result was used to estimate gap duration thresholds.

Two times the standard deviation of the sustained responses was defined as the threshold for significant differences. The gap duration at which the sigmoid function returned this value was defined as the gap-duration threshold of the unit.

Identification of gap duration thresholds in neuronal populations

For population analysis, principal components analysis was applied to reduce the dimensionality of the neuronal population data. Responses from -100 ms to 900 ms after the onset of the first noise were averaged across trials with the same gap durations. The averaged responses were then concatenated for analysis. The first three principal components were used to reconstruct the trajectory of the neuronal population response.

To compare gap duration threshold differences between groups at the neuronal population level, both the distance and the area of the population trajectory representing the response to the first and second noise were calculated. Principal components analysis was performed on 50-unit subgroups that were randomly selected from the original unit pool to ensure that differences in the total number of units per group did not bias population trajectory measures. The trajectory distance was calculated by accumulating the Euclidean distances between consecutive time points. The area of the trajectory was estimated as the accumulated area formed between each pair of time points. This analysis was repeated 100 times for between-group comparisons, with different random selections of 50 units from each group.

For analysis of gap duration sensitivity, the population trajectory distance (or area) for the post-gap noise burst was divided by the trajectory distance (or area) for the pre-gap noise burst. This ratio measure provided a measure of gap duration sensitivity at the neuronal population level that was robust to differences between groups in neuronal responsiveness to noise. This approach, together with the use of sound stimuli adjusted in loudness to compensate for hearing loss on an animal-by-animal basis, ensured that differences in hearing thresholds between animal groups could not account for observed differences in auditory cortical temporal acuity measures.

Results

Malleus removal surgery at P11 in WT mice mimicked hearing loss in *Df1*/+ mice

Like human 22q11.2 deletion carriers, *Df1*/+ mice exhibit a complex hearing phenotype with high inter-individual and even inter-ear variability [13,14]. More than half of *Df1/+* mice have mild to moderate hearing loss in one or both ears [14,15,26]. Hearing loss in *Df1*/+ mice arises primarily from increased risk for otitis media (middle-ear inflammation) as a result of hypoplastic Eustachian tube muscles which reduce the patency of the Eustachian tube [17]. Inflammation and effusion in the middle ear disrupt sound-evoked vibration of the ossicles, causing conductive hearing loss (Figure 1B; compare to Figure 1A showing normal ear). In affected *Df1/+* mice, hearing loss is typically evident soon after ear opening at P11 and persists through adulthood [26].

To mimic a similarly early-onset and persistent conductive hearing loss in WT mice, we removed the malleus bone in P11 WT mouse pups to disrupt sound transduction (Figure 1C-D) [18,19]. To evaluate the severity of hearing loss caused by malleus removal surgery (MRS), we measured click-evoked auditory brainstem responses (ABRs) in separate cohort of mice, including *Df1*/+ mice (n = 15), WT mice with MRS (WT HL, n = 11) and WT mice with sham surgery (WT NH, n = 6) during development (Figure 1E). We classified an ear as having hearing loss (HL) if the click-evoked ABR was higher than 42 dB SPL (2.5 standard deviations above the mean estimated from hearing thresholds of WT ears with sham surgery); otherwise, the ear was classified as normal hearing (NH). To quantify the effects of malleus removal surgery, we grouped ears into *Df1*/+ HL, *Df1*/+ NH, WT HL and WT NH groups. By definition, then, ears in *Df1*/+ HL and WT HL groups had elevated hearing thresholds compared to those in *Df1*/+ NH and WT NH groups (Week 8: *Df1*/+ HL 59.00 ± 2.73 dB SPL, *Df1*/+ NH 32.50 ± 1.12 dB SPL, WT HL 54.00 ± 4.23 dB SPL, WT NH 35.00 ± 2.24 dB SPL; see Supplementary Table 1for hearing thresholds at other ages). No significant differences in hearing thresholds were seen between *Df1*/+ HL and WT HL groups, nor between *Df1*/+ NH and WT NH groups (Week 8, Kruskal-Wallis test, $H_{(3, 46)} = 24.70$, $p < 0.001$, post-hoc, $p_{Df1/+\ HL\ -\ Df1/NH} < 0.001$, $p_{WT\text{-}HL\ -\ WT\ NH} = < 0.001$, $p_{Df1/+\ HL\ -\ WT\ HL} = 0.22$, $p_{Df1/+\ NH\ -\ WT\ NH} = 0.76$). Tone-evoked ABRs revealed similarly increased thresholds across frequencies, consistent with the expected features of conductive hearing loss (Figure 1E). In summary, malleus removal surgery or sham surgery at P11 in WT mice produced hearing phenotypes in WT HL and WT NH mice comparable to those observed in *Df1*/+ HL and *Df1/+* NH mice, respectively.

Intracranial recording of single-unit responses to gap-in-noise stimuli reveals effects of both genotype and hearing phenotype on neural sensitivity to noise transients

We then deployed a 2x2 design to study neuronal responses in mice with different genetic background and hearing sensitivities, recording hearing thresholds for each ear and auditory cortical activity in a total of 17 WT mice that underwent malleus removal or sham surgery and 12 *Df1/+* mice with or without naturally occurring hearing impairment. For analyses reported here, we focused on the subset of animals with equivalent hearing thresholds in the two ears or better hearing in the left ear, which was contralateral to the hemisphere used for cortical recording (Figure 2A; *Df1*/+ HL: *Df1*/+ mice with

both ears having hearing loss, n = 2; *Df1*/+ NH: *Df1*/+ mice with both ears normal hearing, n = 5; WT HL: WT mice with malleus removal surgery in both ears, n = 6; WT NH: WT mice with sham surgery in both ears, n = 10). Neural responses were recorded from the right primary auditory cortex using Neuropixels 1.0 probes while the awake mice passively listened to gap-in-noise stimuli (Figure 2B-C).

Noise levels were set to 20 dB above the threshold of the better hearing ear to prevent overstimulation to the animals. Gap-in-noise stimuli consisted of a first 250-ms noise and a second 100-ms noise separated by a silent gap with duration of 0, 1, 2, 4, 8, 16, 32, 64, 128 or 256 ms. Primary auditory units showed various responses to the gap-in-noise stimuli, including transient responses to noise onset or offset and sustained responses to noise (Figure 2D). These transient responses to the offset of the first noise and/or the onset of the second noise gradually emerged with increasing gap durations, indicating the detection of the gap.

We then quantified the proportion of units with different transient responses to noise onset or noise offset (Figure 2E). All units that passed the physiological criteria for primary auditory units (see Methods) were clustered into units with only onset responses, units with only offset responses, units with both responses and units without transient responses (Figure 2F). These four clusters were distributed differently between animal groups ($\chi^2_{(9, 1052)} = 26.93$, $p = 0.0014$). The group differences appeared to be driven primarily by differences between genotypes for mice with normal hearing: *Df1*/+ NH mice had a higher percentage of units with only onset responses and WT NH mice had a lower percentage of those units, while distributions of neurons with onset-only, offset-only, both or neither transient responses were relatively similar in WT HL and *Df1/*+ HL mice. Thus, proportions of auditory responsive neurons with sensitivity to sound onsets and offsets depended on both genotype and hearing phenotype.

Robust measurement of single-unit gap duration thresholds shows both hearing loss and 22q11.2 deletion are associated with temporal processing deficits

At the single-unit level, gap duration thresholds (GDTs) are often measured purely based on the onset responses to the second noise, ignoring the potential contribution of the offset responses to the first noise [27,28]. Here, we proposed a new method for analyzing GDTs at the single-unit level that utilized all transient and other responses within and immediately following the gap. This method is general and robust enough that it can easily be applied to analysis of temporal acuity in other brain areas and sensory systems.

GDTs for single units were measured by comparing the deviance of neural responses around the gap in different gap conditions to the sustained responses in the 0-ms (no gap) condition (Figure 3A-B; see Methods and Supplementary Figure 1 for more details). We defined the analysis period for gap detection as extending from the start of the gap to the end of the second noise. We then calculated the mean and standard deviation over time in bin-by-bin firing rates in this analysis period for the 0-ms gap condition (i.e., last 100 ms of the 350 ms continuous noise), and the root-mean-squared deviance (RMSD) over time from this mean for the analysis period in other gap conditions. We fitted a sigmoidal function to these RMSD values as a function of gap duration, since the RMSD would be expected to

317 rise rapidly and then level off as gap duration increased. We then defined GDTs for the unit as the gap
318 duration at which the sigmoidal fit exceeded 2 times the standard deviation over time of the neural
319 responses in analysis period for the 0-ms (no gap) condition, thereby taking into account that the
320 variance in the neuron's response to sustained noise affects the reliability of gap detection at the
321 single-unit level.

322 This analysis revealed that GDTs of auditory cortical neurons in WT HL mice were the longest of any
323 mouse group and significantly different from those in WT NH mice, indicating effects of hearing loss.
324 Meanwhile, GDTs of units recorded in *Df1/+* NH mice were mildly elevated compared to those in WT
325 NH mice, revealing effects of the 22q11.2 deletion. Surprisingly, however, no differences were
326 detectable when comparing single-unit GDTs between *Df1/+* HL and *Df1/+* NH mice, even though
327 GDTs were longer in *Df1/+* HL than WT NH mice (Kruskal-Wallis test, $H_{(3, 630)} = 46.56$, $p < 0.001$, post-
328 hoc tests, $p_{Df1/+\ HL\text{-}Df1/+\ NH} = 0.58$, $p_{WT\ HL\text{-}WT\ NH} < 0.001$, $p_{Df1/+\ HL\text{-}WT\ HL} = 0.027$, $p_{Df1/+\ NH\text{-}WT\ NH} = 0.0028$,
329 $p_{Df1/+\ HL\text{-}WT\ NH} = 0.020$; Figure 3C). Thus, single-unit measures of GDTs revealed that temporal acuity of
330 neurons in the auditory cortex was dependent on both the hearing phenotype and the genotype of the
331 mouse. In further analysis of units with onset and/or offset responses, we found that in normal hearing
332 mice (both WT NH and *Df1/+* NH groups), units with only-onset or both onset and offset responses
333 had shorter GDTs than units with only-offset responses (Supplementary Figure 2).

334 We also separated neurons based on their waveform features into putative excitatory neurons
335 (regular-spiking units, RS) and putative parvalbumin-positive (PV^+) interneurons (fast-spiking units,
336 FS) (Supplementary Figure 3). Surprisingly, given evidence for higher temporal acuity in PV^+ cells than
337 in pyramidal neurons [28], we found no significant differences in GDT distributions between fast-spiking
338 and regular-spiking in either of the WT groups (Mann-Whitney U test; WT HL, $U_{(166, 128)} = 10679$, $p_{WT\ HL}$
339 $= 0.94$; WT NH, $U_{(93, 86)} = 4185$, $p_{WT\ NH} = 0.59$; Figure 3D), even though fast-spiking units were more
340 sensitive to transient onset and offset events than regular-spiking units. In contrast, *Df1*/+ mice with
341 normal hearing or hearing loss had divergent GDTs between RS and FS units (Mann-Whitney U test;
342 *Df1*/+ HL, $U_{(28, 36)} = 663$, $p_{Df1/+\ HL} = 0.032$; *Df1*/+ NH, $U_{(25, 36)} = 600$, $p_{Df1/+\ NH} = 0.028$). Interestingly,
343 GDTs of RS units in both *Df1/+* HL and *Df1/+* NH mice were abnormally elevated related to those in
344 WT NH mice (and similar to those in WT HL mice), while GDTs of FS units in both *Df1/+* HL and *Df1/+*
345 NH mice were similar to those in WT NH mice.

346 Novel measures of gap duration thresholds for neuronal population responses reveal 347 only effects of hearing loss

348 Next we asked whether differences between animal groups in single-unit GDT distributions were also
349 evident at the level of neuronal population dynamics. We applied principal component analysis (PCA)
350 to reduce the dimensionality of the neuronal population and used the top three principal components
351 (PCs) for representation (Figure 4A). The dynamics of PCs mainly revealed transient responses to
352 noise onset and noise offset (Figure 4B). The most significant between-group differences appeared in
353 PC1; responses to sustained noise were stronger in mice with hearing loss.

To better visualize the dynamics of population responses to gap-in-noise stimuli, we reconstructed the trajectory of neuronal responses to gap-in-noise stimuli in PC1-3 space (Figure 4C). When the noise was present, the trajectory moved outward quickly and then stabilized at an evoked location. Once the noise was off, the trajectory gradually returned to the starting point. When the second noise burst occurred, the trajectory rebounded. The extent of these rebound activities was dependent on the gap length; smaller gaps resulted in minimal rebound activity, whereas extended gaps led to increasingly pronounced rebound activities to the second noises.

We used the distance of the trajectory and the area covered by the trajectory to approximate the gap duration threshold of the neuronal populations recorded in each animal group (Figure 4D and 4E). The trajectory distance was calculated as the cumulative sum of the Euclidean distances between consecutive time points. The area covered by the trajectory was estimated by the cumulative sum of curved triangles formed along the trajectory. Both the trajectory distance and trajectory area indicated that at the neuronal population level, gap duration thresholds in mice with normal hearing were shorter compared to those with hearing loss, regardless of their genetic background. Thus, effects of hearing loss on auditory cortical temporal acuity dominated effects of genotype at the neuronal population level.

Discussion

Auditory cortical dysfunction is commonly recognized as an endophenotype of psychosis [1], and provides a window for investigating how multiple risk factors contribute to the generation of neuropathology in psychiatric disease. In this study, we examined auditory cortical abnormalities associated with hearing loss and the 22q11.2 deletion using gap-in-noise stimuli as a sensitive index of temporal dynamics in the auditory cortex. We first showed that malleus removal surgery in WT mice induced conductive hearing loss comparable to that observed in a subset of *Df1/+* mice. We then established robust methods to quantify duration thresholds for responses to a brief gap in noise at both the single-unit and neuronal population levels, enabling precise assessment of auditory cortical temporal acuity across mice with different genetic backgrounds and hearing sensitivities. Finally, we deployed these methods in a 2x2 experimental design, to disentangle the effects of hearing loss and the *Df1* deletion on auditory cortical temporal acuity.

The results indicated that hearing loss and the *Df1/+* deletion alter temporal dynamics in the auditory cortex both independently and jointly. Hearing loss impaired auditory cortical temporal acuity at both the single-unit and neuronal population levels in WT mice, even though sound intensity was adjusted to be constant relative to hearing threshold for each mouse. In contrast, the *Df1* deletion alone caused a more modest disruption of cortical temporal acuity, and its effects were detectable only at the single-unit level. Importantly, the effects of the experiential and genetic factors differed in their cell-type specificity: hearing loss impaired gap duration thresholds in both putative excitatory and putative inhibitory neurons, whereas the *Df1* deletion selectively affected putative excitatory neurons. The interactions between the two risk factors appeared more complex, in that effects of hearing loss in *Df1/+* mice were evident only at the neuronal population level; there were no clear differences in

392 single-unit gap duration thresholds observed when comparing *Df1*/+ HL and *Df1*/+ NH mice. Together,
393 these observations suggest that hearing loss and the 22q11.2 deletion disrupt cortical temporal acuity
394 through distinct neural mechanisms.

395 Our data align with previous behavioural and neurophysiological studies showing that hearing loss
396 impairs gap detection [10]. Young adults with normal hearing can detect silent gaps as short as 2-ms in
397 continuous noise, and hearing loss elevates the detection thresholds by a factor of two or more.
398 Similar gap detection threshold shifts caused by hearing loss have also been reported in animal
399 models [27,29]. The differences we observed in gap duration thresholds between mouse groups with and
400 without hearing loss were similar in magnitude to those reported in previous behavioural and
401 neurophysiological studies in rodents. In contrast to a report that PV^+ inhibitory neurons have shorter
402 gap duration thresholds [28], in WT mice no clear differences in gap duration thresholds were observed
403 between fast-spiking units and regular spiking units, and hearing loss had similar impact on these two
404 neuron subtypes.

405 The influence of the 22q11.2 deletion on auditory cortical temporal processing can be summarised in
406 three key observations. First, at the single-unit level, gap duration thresholds were mildly elevated
407 even in *Df1*/+ mice with normal hearing, relative to WT mice with normal hearing. This mild impairment
408 of cortical temporal acuity in *Df1/*+ mice might arise from synaptic changes caused by
409 haploinsufficiency of genes located in the deletion region [30,31]. Second, an unusually high proportion of
410 auditory cortical units in *Df1*/+ mice with normal hearing had onset-only responses to noise bursts.
411 Since units with onset-only responses also tended to have the shortest gap duration thresholds, this
412 increase in the proportion of cells with onset-only transient responses seems more likely to be a
413 compensating than contributing factor for auditory temporal processing deficits. Third, and most
414 strikingly, the *Df1* deletion was associated with divergence in temporal acuity between neuron
415 subtypes: gap duration thresholds were longer in regular-spiking than fast-spiking units in *Df1/*+ mice
416 with or without hearing loss. Longer gap duration thresholds in regular-spiking units (putative
417 pyramidal excitatory neurons) may be related to reduced evoked excitability [32] and disrupted
418 thalamocortical connections [33] in mouse models of 22q11.2 Deletion Syndrome. Fast-spiking units
419 (putative PV^+ inhibitory neurons) appeared more robust in *Df1/*+ mice, with shorter gap duration
420 thresholds that were similar to those observed in WT mice with normal hearing and minimally affected
421 by hearing loss.

422 The combined effects of hearing loss and *Df1* deletion were more complicated. We found that units
423 with only onset responses or both onset and offset responses had shorter gap duration thresholds and
424 were more strongly impacted by both hearing loss and genetic risk factors than units with only offset
425 responses. Differences in temporal acuity and risk factor sensitivity of onset- and offset-sensitive
426 neurons might reflect distinct underlying pathways and mechanisms for generation of onset and offset
427 responses [25,34]. At the neuronal population level, no abnormalities in gap duration thresholds were
428 evident in *Df1/*+ mice with normal hearing compared to WT mice with normal hearing, while population
429 activity trajectories evoked by brief gaps in noise were impaired in both WT HL and *Df1*/+ HL groups.
430 This observation might also reflect compensation, at the cortical circuit and neuronal population level,

for subtle defects in auditory cortical temporal processing associated with the Df1 deletion. However, it might also reflect differences in sensitivity of population versus single-unit measures of auditory temporal acuity. Further experiments, including developmental studies, would be necessary to resolve this issue.

In conclusion, this work illustrates how animal models can be used to address questions about the role of comorbidities in psychiatric disease that are difficult or impractical to address in humans. In humans with the 22q11.2 deletion, it is not known whether comorbid hearing loss exacerbates risk of developing psychiatric disease, although hearing loss is known to be a risk factor for psychosis in the general population. In mice, we were able to compare genetically homogeneous groups of mice with and without hearing loss and with and without a mouse homologue of the 22q11.2 deletion, to disentangle effects of experiential and genetic risk factors with a precision that would be impossible to achieve even in studies of human siblings or twins. We analyzed effects of these risk factors on a sensitive measure of auditory brain function: cortical temporal dynamics evoked by brief silent gaps in noise. Results showed that the 22q11.2 deletion alone alters auditory cortical temporal processing, but effects of hearing loss are more profound at both the single-unit and neuronal population levels. Thus, these findings provide a mechanistic proof-of-concept that hearing loss comorbidity could be a "second hit" for cortical dysfunction in psychiatric disease.

Acknowledgements

We thank Eleanor Benoit for her assistance with data collection. We are grateful to Dan Sanes for providing detailed advice on malleus removal surgery in mice. We also thank Elvira Bramon, Peter Keating, and Nick Lesica for their contributions to supervision of Chen Lu's PhD research. This work was supported by the UCL Institute for Mental Health (Small Grant 2022 to JFL) and the UK Medical Research Council (grant MR/P006221/1 to JFL), and also received support from the NIHR UCLH Biomedical Research Centre Hearing Health Theme.

Author contributions

CL: conceptualization, methodology, software, investigation, formal analysis, visualization, writing.
JFL: conceptualization, resources, writing, supervision, funding acquisition.

Disclosures

The authors report no conflicts of interest.

Data Availability

Raw data (in Neurosciences Without Borders format) and/or analysis code (in Python) are available from the authors upon request.

References

1. Javitt, D. C. & Sweet, R. A. Auditory dysfunction in schizophrenia: integrating clinical and basic features. *Nat. Rev. Neurosci.* **16**, 535–550 (2015).

2. Viertiö, S., Perälä, J., Saarni, S., Koskinen, S. & Suvisaari, J. Hearing loss in persons with psychotic disorder–findings from a population-based survey. *Schizophrenia Research* **159**, 309–311 (2014).

3. Saperstein, A. M., Meyler, S., Golub, J. S. & Medalia, A. Correlates of hearing loss among adults with schizophrenia. *Schizophrenia Research* **257**, 1–4 (2023).

4. Linszen, M. M. J., Brouwer, R. M., Heringa, S. M. & Sommer, I. E. Increased risk of psychosis in patients with hearing impairment: Review and meta-analyses. *Neurosci. Biobehav. Rev.* **62**, 1–20 (2016).

5. Tallal, P. & Piercy, M. Defects of Non-Verbal Auditory Perception in Children with Developmental Aphasia. *Nature* **241**, 468–469 (1973).

6. Merzenich, M. M. *et al.* Temporal Processing Deficits of Language-Learning Impaired Children Ameliorated by Training. *Science* **271**, 77–81 (1996).

7. Mauk, M. D. & Buonomano, D. V. THE NEURAL BASIS OF TEMPORAL PROCESSING. *Annual Review of Neuroscience* **27**, 307–340 (2004).

8. Iliadou, V. V. *et al.* Is central auditory processing disorder present in psychosis? *Am J Audiol* **22**, 201–208 (2013).

9. Moschopoulos, N., Nimatoudis, I., Kaprinis, S., Sidiras, C. & Iliadou, V. Auditory processing disorder may be present in schizophrenia and it is highly correlated with formal thought disorder. *Psychiatry Research* **291**, 113222 (2020).

10. Fitzgibbons, P. J. & Wightman, F. L. Gap detection in normal and hearing-impaired listeners. *J. Acoust. Soc. Am.* **72**, 761–765 (1982).

11. Boot, E. *et al.* Updated clinical practice recommendations for managing adults with 22q11.2 deletion syndrome. *Genetics in Medicine* **25**, 100344 (2023).

12. Bassett, A. S. & Chow, E. W. C. Schizophrenia and 22q11.2 deletion syndrome. *Curr Psychiatry Rep* **10**, 148–157 (2008).

13. Verheij, E., Derks, L. S. M., Stegeman, I. & Thomeer, H. G. X. M. Prevalence of hearing loss and clinical otologic manifestations in patients with 22q11.2 deletion syndrome: A literature review. *Clinical Otolaryngology* **42**, 1319–1328 (2017).

14. Fuchs, J. C. *et al.* Hearing loss in a mouse model of 22q11.2 deletion syndrome. *PLoS ONE* **8**, e80104 (2013).

15. Lu, C. & Linden, J. F. Auditory evoked-potential abnormalities in a mouse model of 22q11.2 Deletion Syndrome and their interactions with hearing impairment. *Transl Psychiatry* **15**, 1–13 (2025).

16. Lindsay, E. A. *et al.* Congenital heart disease in mice deficient for the DiGeorge syndrome region. *Nature* **401**, 379–383 (1999).

17. Fuchs, J. C., Linden, J. F., Baldini, A. & Tucker, A. S. A defect in early myogenesis causes otitis media in two mouse models of 22q11.2 deletion syndrome. *Human Molecular Genetics* **24**, 1869–1882 (2015).

18. Tucci, D. L., Cant, N. B. & Durham, D. Conductive hearing loss results in a decrease in central auditory system activity in the young gerbil. *The Laryngoscope* **109**, 1359–1371 (1999).

19. Mai, J. *et al.* Sound-seeking before and after hearing loss in mice. *Sci. Rep.* **14**, 19181 (2024).

20. Buccino, A. P. *et al.* SpikeInterface, a unified framework for spike sorting. *eLife* **9**, e61834 (2020).

21. Pachitariu, M., Steinmetz, N., Kadir, S., Carandini, M. & Kenneth D., H. *Kilosort: Realtime Spike-Sorting for Extracellular Electrophysiology with Hundreds of Channels*. http://biorxiv.org/lookup/doi/10.1101/061481 (2016) doi:10.1101/061481.

22. Resnik, J. & Polley, D. B. Fast-spiking GABA circuit dynamics in the auditory cortex predict recovery of sensory processing following peripheral nerve damage. *eLife* **6**, e21452 (2017).

23. Li, L. -y. *et al.* Differential receptive field properties of parvalbumin and somatostatin inhibitory neurons in mouse auditory cortex. *Cereb Cortex* **25**, 1782–1791 (2015).

24. Sun, S. H. *et al.* Analysis of extracellular spike waveforms and associated receptive fields of neurons in cat primary visual cortex. *The Journal of Physiology* **599**, 2211–2238 (2021).

25. Kopp-Scheinpflug, C., Sinclair, J. L. & Linden, J. F. When sound stops: Offset responses in the auditory system. *Trends in Neurosciences* **41**, 712–728 (2018).

26. Zinnamon, F. A. *et al.* Increased Central Auditory Gain and Decreased Parvalbumin-Positive Cortical Interneuron Density in the *Df1/+* Mouse Model of Schizophrenia Correlate With Hearing Impairment. *Biol. Psychiatry Glob. Open Sci.* **3**, 386–397 (2023).

27. Green, D. B., Mattingly, M. M., Ye, Y., Gay, J. D. & Rosen, M. J. Brief Stimulus Exposure Fully Remediates Temporal Processing Deficits Induced by Early Hearing Loss. *J. Neurosci.* **37**, 7759–7771 (2017).

28. Keller, C. H., Kaylegian, K. & Wehr, M. Gap encoding by parvalbumin-expressing interneurons in auditory cortex. *Journal of Neurophysiology* **120**, 105–114 (2018).

29. Radziwon, K. E., Stolzberg, D. J., Urban, M. E., Bowler, R. A. & Salvi, R. J. Salicylate-Induced Hearing Loss and Gap Detection Deficits in Rats. *Front. Neurol.* **6**, (2015).

30. Zinkstok, J. R. *et al.* Neurobiological perspective of 22q11.2 deletion syndrome. *The Lancet Psychiatry* **6**, 951–960 (2019).

31. Nehme, R. *et al.* The 22q11.2 region regulates presynaptic gene-products linked to schizophrenia. *Nat Commun* **13**, 3690 (2022).

32. Khan, T. A. *et al.* Neuronal defects in a human cellular model of 22q11.2 deletion syndrome. *Nat Med* **26**, 1888–1898 (2020).

33. Chun, S. *et al.* Specific disruption of thalamic inputs to the auditory cortex in schizophrenia models. *Science* **344**, 1178–1182 (2014).

34. Scholl, B., Gao, X. & Wehr, M. Nonoverlapping sets of synapses drive on responses and off responses in auditory cortex. *Neuron* **65**, 412–421 (2010).

Figure

Figure 1

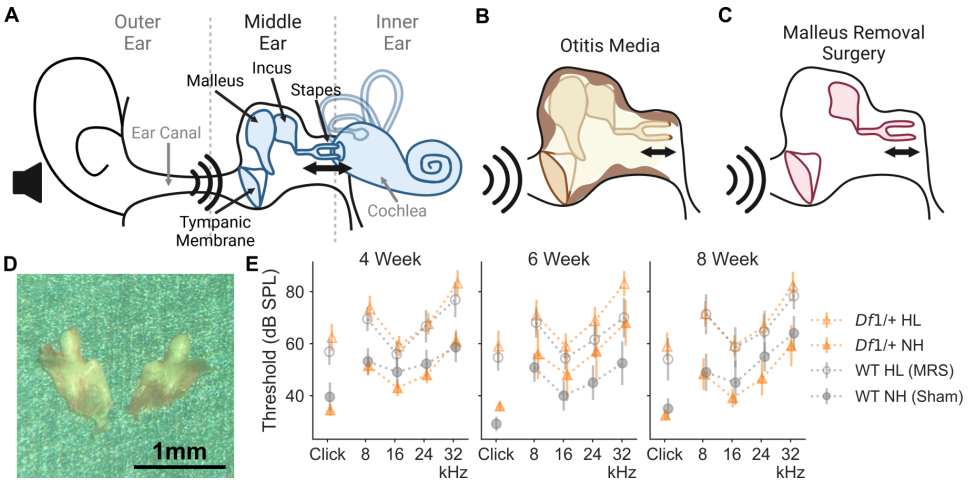

Figure 1. Malleus removal surgery in P11 WT mice mimics early conductive hearing loss observed in *Df1*/+ mice.

(A) Anatomy of the mouse ear. The ossicular chain in the middle ear transmits sound vibrations to the inner ear via the connection of the malleus, incus, and stapes. **(B)** Hearing loss in *Df1/+* mice is primarily conductive, resulting from otitis media (inflammation and effusion in the middle ear) which disrupts ossicle movement and sound transmission. **(C)** Malleus removal surgery also disrupts sound transmission through the middle ear to produce conductive hearing loss. **(D)** Malleus bones dissected from a P11 WT mouse. **(E)** Click-evoked auditory brainstem response (ABR) thresholds show that malleus removal surgery in P11 WT mice caused conductive hearing loss similar to that observed in *Df1/+* mice. Orange dashed line, *Df1/+* mice with hearing loss (*Df1*/+ HL); orange solid line, *Df1/+* mice with normal hearing (*Df1*/+ NH); gray dashed line, WT mice with hearing loss (WT HL); gray solid line, WT mice with normal hearing (WT NH). Error bars represent mean ± 2 SEM.

555 **Figure 2**

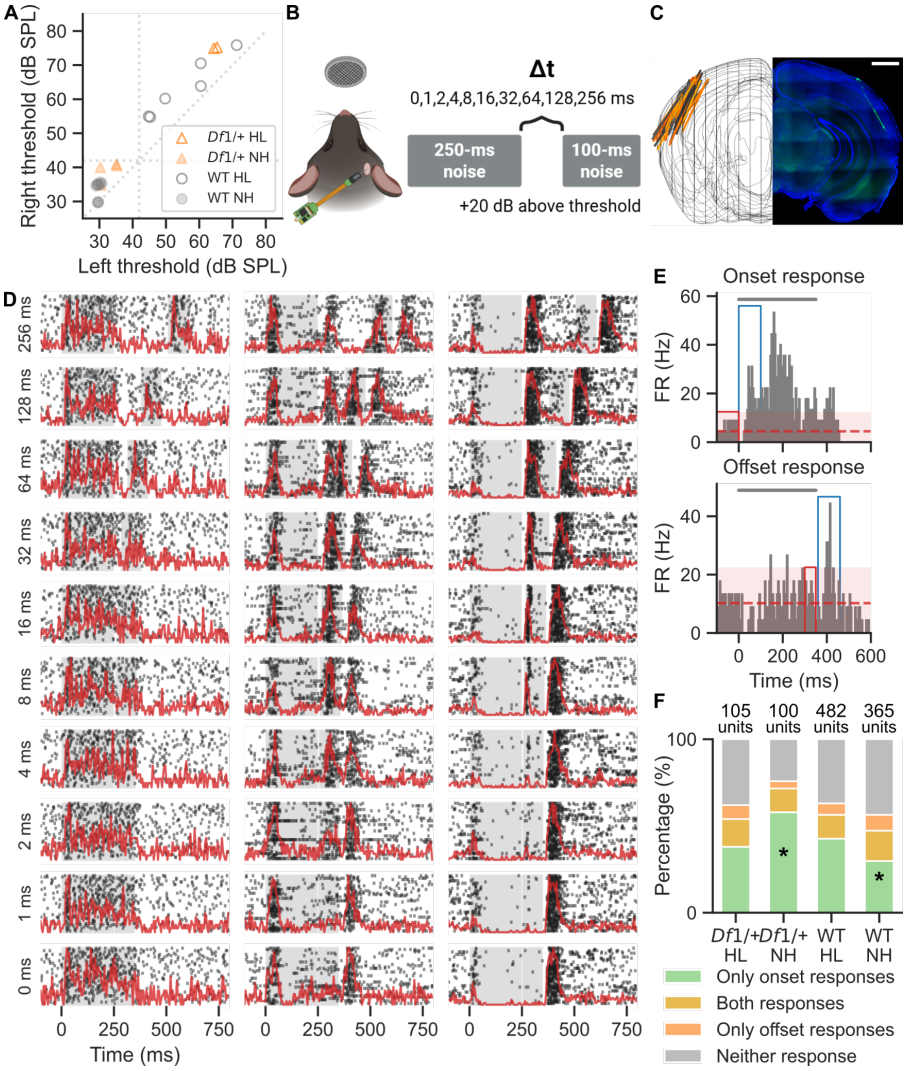

556

557 **Figure 2. Neuropixels recordings reveal diverse neuronal responses to gap-in-noise stimuli in**
558 **the auditory cortex of awake mice, and differences between animal groups in neuronal**
559 **sensitivity to sound onsets and offsets.**

560 **(A)** Hearing thresholds were measured in each ear of each mouse prior to auditory cortical recording.
561 Mice with worse hearing in the left ear (not shown) were excluded from the study, to avoid
562 understimulating the right (contralateral) auditory cortex where neuronal responses were recorded.
563 Remaining animals were grouped into *Df1*/+ HL (unfilled orange triangle, n = 2), *Df1*/+ NH (filled
564 orange triangle, n = 5), WT HL (unfilled grey circle, n = 6) and WT NH (filled grey circle, n=10). **(B)**
565 Single-unit activities were recorded using acute Neuropixels 1.0 probes in the right auditory cortex of
566 awake passively listening mice presented with gap-in-noise stimuli of varying gap durations. White
567 noise intensity was individually adjusted for each mouse to be 20 dB above the left ear hearing
568 threshold (which was the better-hearing or equivalent-hearing ear for all mice). **(C)** Probe traces in
569 histological sections (right) and reconstructed trajectories (left). Right: green, DiO; blue, DAPI; scale
570 bar, 1 mm. **(D)** Raster plots and peri-stimulus time histograms (PSTHs) show neuronal responses to
571 gap-in-noise stimuli from three example units. Gray area, noise presentation; black dots, spike events;

red line, PSTH. **(E)** Definition of onset and offset responses in single units. The gray histogram represents neural activity surrounding noise presentation (gray bar above). Transient responses were defined as at least two consecutive bins with significant increases in firing rate within the analysis window (blue) relative to the reference window (cyan; nonsignificant range shown in red). To capture suppression in neural firing by sound, significantly reduced responses were included for onset response detection (see Methods). **(F)** Distributions of units with different forms of sensitivity to noise onset and offset transients revealed significant differences between groups, particularly between *Df1*/+ NH and WT NH mice (marked with *) for units with onset-only responses.

Figure 3

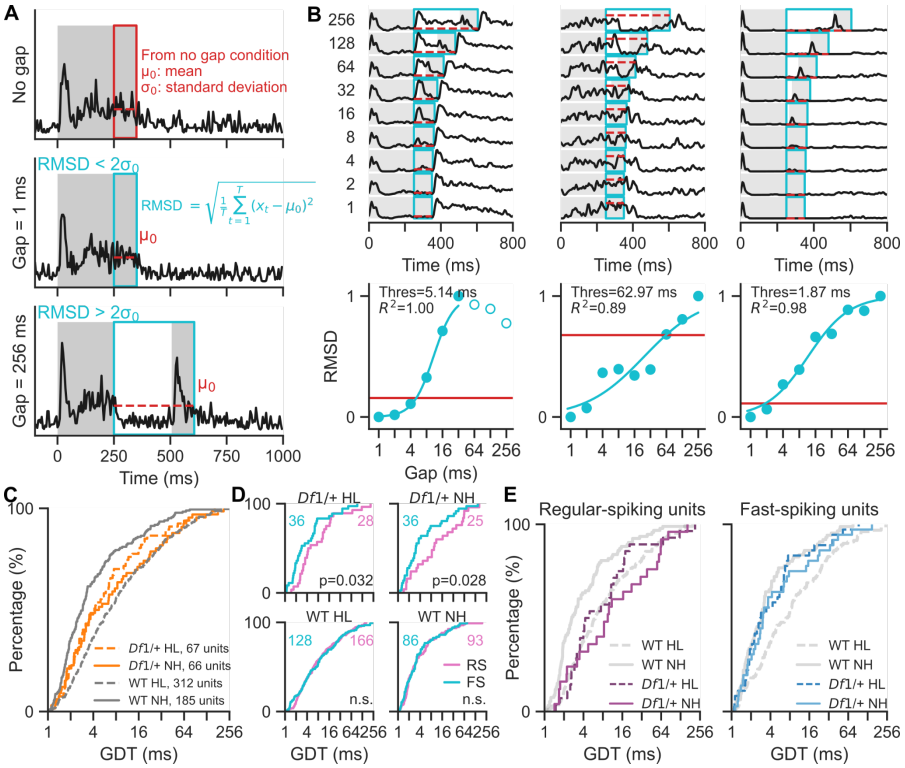

Figure 3. Single-unit gap duration thresholds (GDTs) were longer in mice with hearing loss.

(A) Single-unit GDT was estimated by comparing the root mean squared deviation (RMSD) of neuronal responses in any gap condition to the no-gap condition, over a time period extending from the end of the 250 ms first noise segment to the end of the 100 ms second noise segment. For the no-gap condition (top, red box) this period was a continuation of noise without a silent gap. For gap conditions (middle and bottom, cyan boxes), this period included a silent gap of variable duration. **(B)** Example GDT measurement in three example units. The RMSD of responses to the gap (highlighted with cyan shaded area in the top) was normalized (cyan dots in the bottom) and then fitted with a sigmoid function (cyan curve). The gap duration that corresponded to an RMSD 2 times as large as the standard deviation for the no-gap condition (red line) was defined as the GDT for that unit. Hollow circles represent data points not included in the sigmoid fitting. **(C)** Cumulative distribution functions of GDT for all units. GDTs were longer in units from WT HL mice than WT NH mice. GDTs were also longer in units from *Df1/+* NH mice than WT NH mice. Although GDTs were longer in units from *Df1/+* HL mice than WT NH mice, no significant differences were evident between *Df1/+* HL and *Df1/+* NH animals. **(D)** Cumulative distribution functions of GDT for units that could be classified with over 95% confidence as regular-spiking (RS, pink) or fast-spiking (FS, cyan) units. GDTs of RS units were significantly longer than GDTs of FS units in both *Df1/+* HL and *Df1/+* NH mice. No significant differences were evident between GDTs of RS and FS units in either WT HL or WT NH mice. **(E)** For RS units (left), GDTs were longer in both *Df1/+* HL and *Df1/+* NH mice than in WT NH mice. In contrast, for FS units (right), GDTs in both *Df1/+* HL and *Df1/+* NH mice were similar to FS unit GDTs in WT NH mice.

603 **Figure 4**

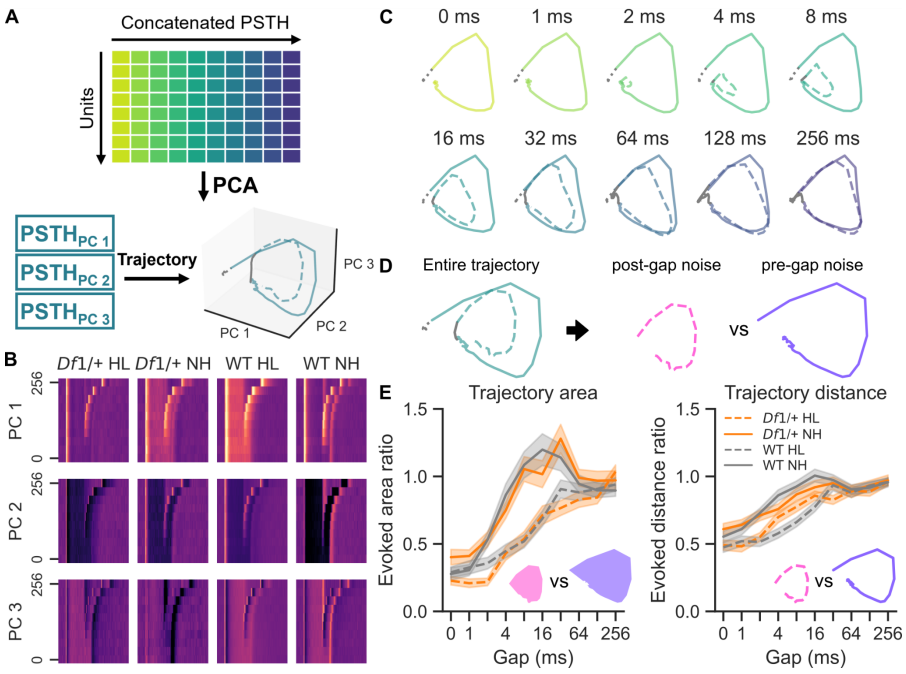

604

605 **Figure 4. Analysis of neuronal population dynamics revealed elevated gap duration thresholds**
606 **in mice with hearing loss.**

607 **(A)** Population activity was analyzed using principal component analysis. PSTHs from different gap
608 duration conditions were concatenated for each neuron and then principal components (PCs)
609 estimated to capture variability across neurons at each time point. Concatenated trial conditions were
610 subsequently unwrapped for display of population trajectories in PC space for different gap conditions.
611 **(B)** The temporal evolution of principal components captured population response dynamics across
612 gap duration conditions in different animal groups. All PC weightings are shown on the same color
613 scale. **(C)** In the space defined by the first three PCs in WT HL mice, trajectories for the second noise
614 burst (colored dashed line) approached those for the first noise burst (colored solid line) as gap
615 duration increased. The trajectory during the gap (solid gray line) was distinct from those during noise
616 periods. **(D)** The area and distance ratios of trajectories evoked by the post-gap noise relative to those
617 evoked by the pre-gap noise were calculated to compare gap-duration sensitivity of the neuronal
618 population across groups. **(E)** Bootstrapped estimates of trajectory area (defined as the sum of
619 triangular areas formed between adjacent timepoints and the baseline starting point) showed that
620 population responses in *Df1*/+ HL and WT HL mice were less sensitive to short gaps in noise than
621 those in *Df1*/+ NH and WT NH mice. Bootstrapped estimates of trajectory distance (defined as the
622 sum of distances between adjacent timepoints) revealed a similar trend toward reduced population
623 sensitivity to short gaps in mice with hearing loss. Shaded areas represent mean ± 3.3 SEM,
624 corresponding to the 99.9% confidence interval.

625 **Figure 5**

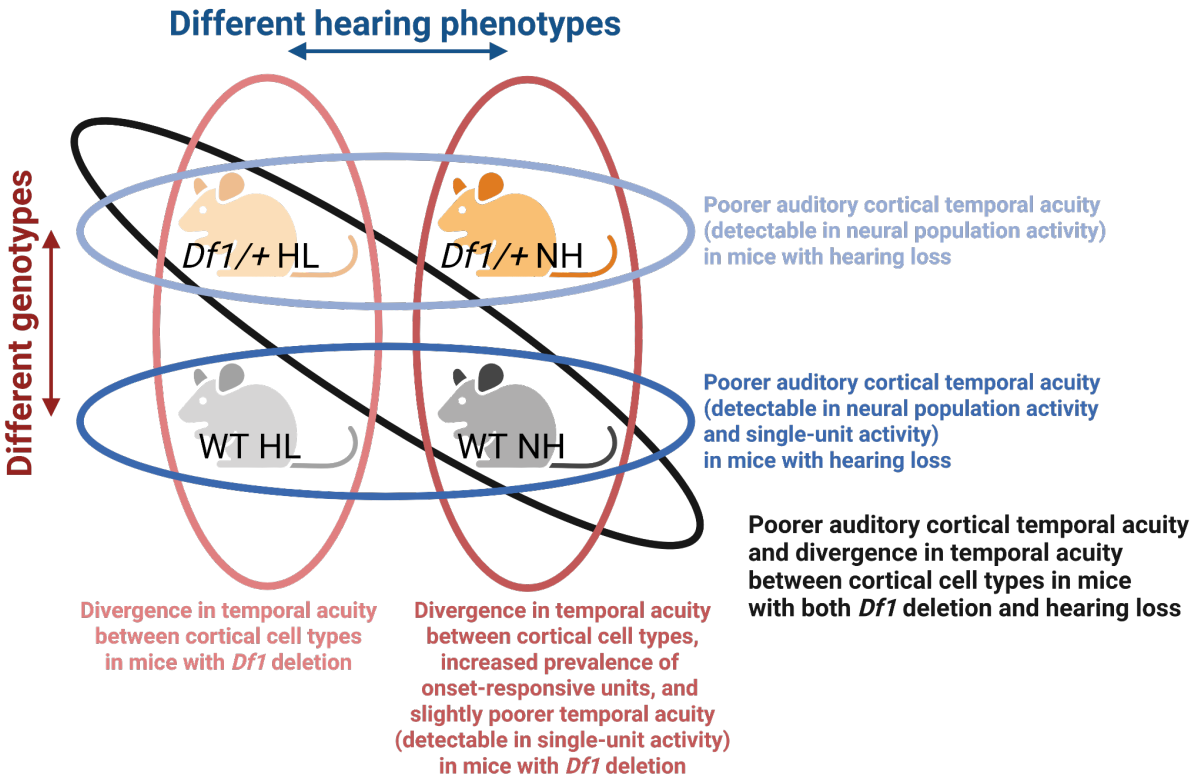

626

627 **Figure 5. Summary of key results.**

628 In *Df1/+* mice with hearing loss, neurophysiological recordings revealed poorer auditory cortical
629 temporal acuity and divergence in temporal acuity between cortical cell types, compared to wildtype
630 mice with normal hearing (black ovals and text). To disentangle the contributions of genotype and
631 hearing phenotype to these cortical abnormalities, we used a 2x2 experimental design. Mice with the
632 *Df1* deletion either had normal hearing (*Df1/+* NH) or naturally occurring hearing loss (*Df1/+* HL).
633 Wildtype mice either had normal hearing following a sham ear surgery at P11 (WT NH) or induced
634 hearing loss following malleus removal surgery at P11 (WT HL), which was performed to mimic the
635 early-onset middle-ear problems known to cause hearing loss in some *Df1/+* mice. Between mouse
636 groups with different hearing phenotypes but the same genotype (light and dark blue ovals and text),
637 the most consistent finding was poorer temporal acuity of neural population activity in mice with
638 hearing loss. More specifically, brief silent gaps in noise evoked smaller excursions in auditory cortical
639 population trajectories in mice with hearing loss than in mice with normal hearing, even though sound
640 levels were adjusted relative to each animal's hearing threshold to ensure similar loudness for all
641 mice. Between mouse groups with different genotypes but the same hearing phenotype (light and dark
642 red ovals and text), the most consistent finding was divergence in temporal acuity between cortical cell
643 types in mice with the *Df1* deletion. More specifically, gap duration thresholds for single-unit responses
644 to brief gaps in noise were longer in regular-spiking (putative excitatory) than fast-spiking (putative
645 inhibitory) units in mice with the *Df1* deletion, while gap duration thresholds were similar for both unit
646 types in WT mice. These results suggest that the 22q11.2 deletion and hearing loss disrupt auditory

647 cortical temporal acuity through different mechanisms. Figure created with BioRender
648 (www.biorender.com).

Supplementary Information

Supplementary Methods

Auditory brainstem response recording

Auditory stimuli were generated at a sample rate of 195,312.5 Hz using a digital signal processor (Tucker Davis Technologies, TDT RX6). The signals were attenuated (TDT PA5), amplified (TDT SA1), and delivered via a free-field speaker (TDT FF1) positioned 10 cm from the tested ear. The speaker output was calibrated to within ± 1.5 dB of the target values (100 or 105 dB SPL) using a free-field 1/4" microphone (G.R.A.S.) placed at the location of the stimulated ear.

Auditory brainstem response (ABR) signals were recorded using subdermal electrodes (Rochester Medical) positioned at the vertex (positive electrode), the bulla of the tested ear (reference electrode), and the olfactory bulb (ground electrode). Data were acquired at a sample rate of 24,414 Hz (TDT RX5) using a low-impedance headstage and signal amplifier (TDT RA4LI and RA16SD, with an overall gain of 20x, and 2.2 Hz - 7.5 kHz filtering), supplemented by a custom low-pass filter designed to remove attenuation switching transients (cutoff at 100 kHz). Stimulus presentation and data acquisition were managed using TDT BrainWare software in combination with custom MATLAB scripts.

Animals were anesthetized with a cocktail solution of ketamine (75 mg/kg body weight) and medetomidine (0.3 mg/kg body weight), administered via intraperitoneal injection. Carprofen (5 mg/kg body weight) was administered subcutaneously for analgesia. Saline or Hartmann's solution (0.1 mL) was administered for hydration. To protect the eyes during the procedure, a liquid gel (Viscotears or GelTears) was applied. The skin was disinfected with 70% ethanol. The body temperature of each mouse was maintained at 37 °C using a homeostatic blanket. Breathing rate and toe-pinch response were monitored frequently to ensure stable anaesthesia. For recovery ABR measurements, animals were administered atipamezole (2 mg/kg body weight) and placed in a warm cage (26-30 °C) until they fully recovered.

The ABR signal was measured as the potential difference between the filtered signals from the vertex electrode and the ear bulla electrode. The signals were filtered using a fifth-order Butterworth band-pass filter with a frequency range of 500–3000 Hz. Averaged ABR signals across different intensity levels were plotted in a stacked format. The hearing threshold was defined as the lowest sound intensity level that evoked an ABR response with at least one deflection larger than 2 standard errors in the pre-stimulus ABR signal.

Supplementary Figures

Supplementary Figure 1

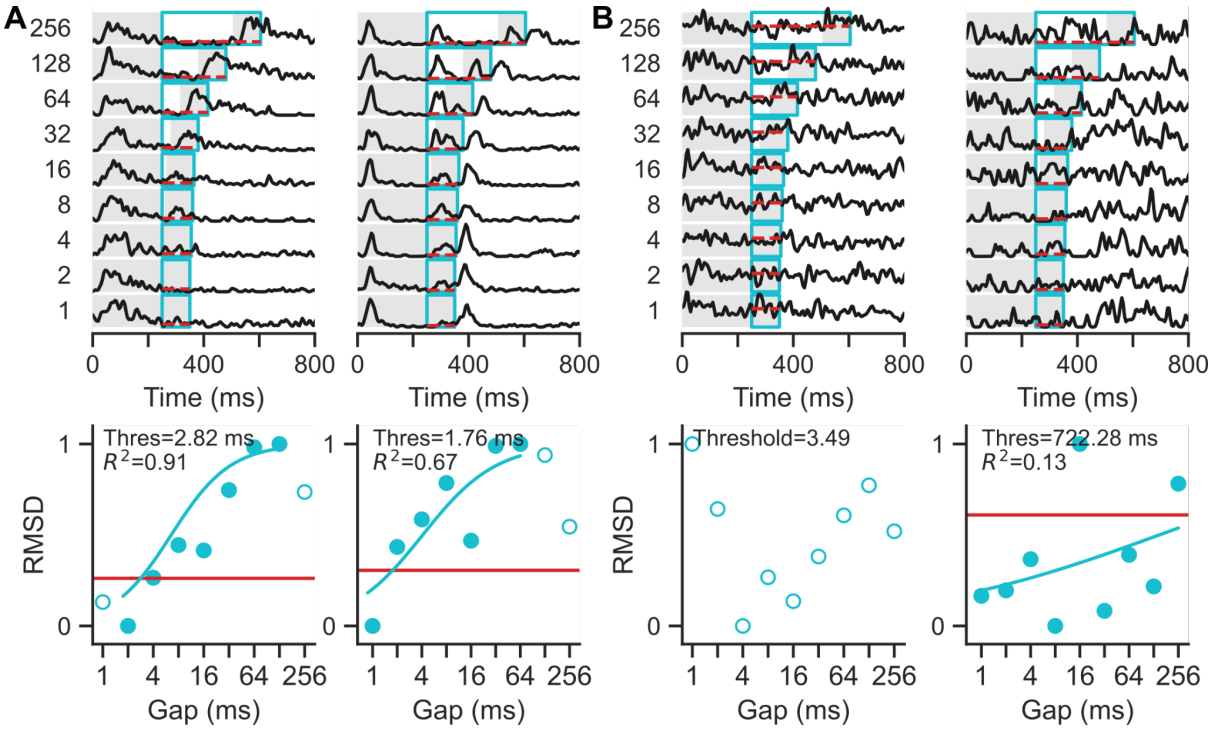

Supplementary Figure 1. Additional examples of single-unit gap duration threshold (GDT) analysis methods. (A) Example units for which data from only a subset of gap durations were included in the sigmoid fit. When RMSD values decreased at longer gap durations (left) or were close to zero for shorter gaps (left and right), the sigmoid fit was performed after excluding these problematic data points (hollow circles). If the sigmoid fit was improved by the data exclusion, then the gap duration thresholds were estimated using this modified sigmoid fit. **(B)** Example units for which no gap detection thresholds could be identified.

690 **Supplementary Figure 2**

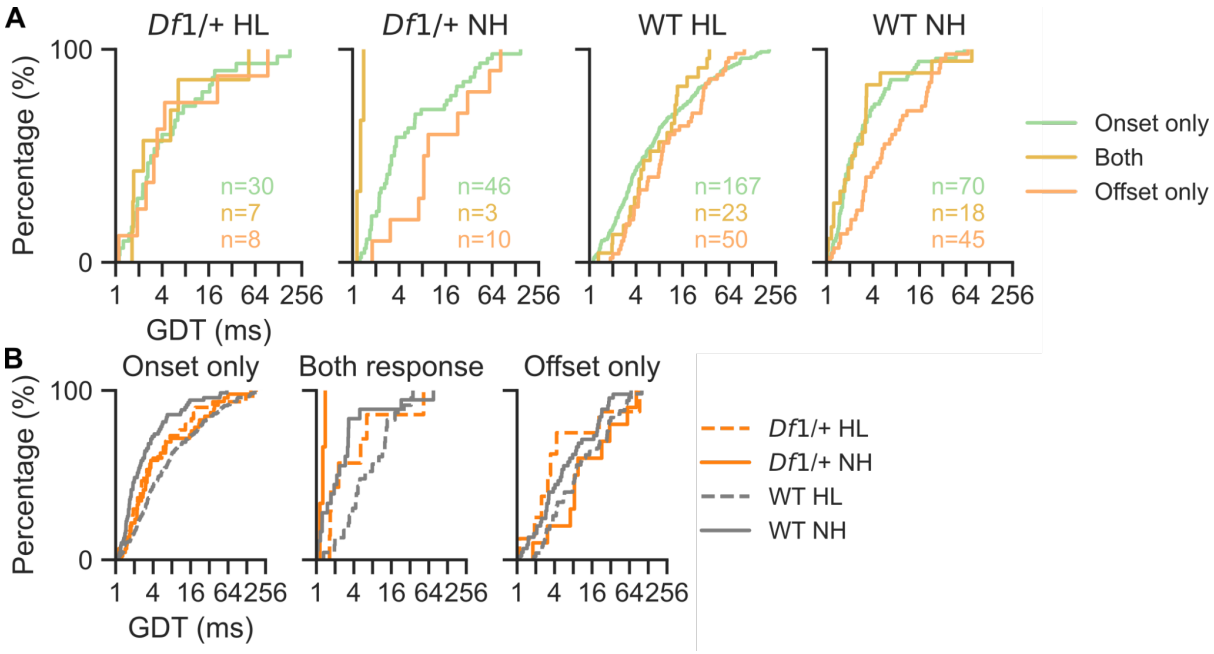

691

692 **Supplementary Figure 2. Distribution of gap duration thresholds (GDTs) in units with different**
693 **onset and offset responses. (A)** In normal hearing mice (*Df1/+* NH and WT NH), units with only
694 offset responses had longer GDTs compared to units with only onset responses or with both
695 responses (two-sample Kolmogorov-Smirnov test, units with only offset versus units with only onset
696 and units with both onset and offset, $p_{Df1/+\ HL}$= 0.97, $p_{Df1/+\ NH}$= 0.015, $p_{WT\ HL}$= 0.073, $p_{WT\ NH}$ = 0.001). **(B)**
697 For comparison across animal groups, units with onset-only responses in WT NH mice had the
698 shortest GDTs while those in WT HL mice had the longest (Kruskal-Wallis test, $p < 0.001$; significant
699 p-values in post-hoc tests, $p_{WT\ HL\text{-}WT\ NH} < 0.0083$, $p_{Df1/+\ NH\text{-}WT\ NH} < 0.001$). Units with both onset and
700 offset responses showed similar trends between WT NH and WT HL mice (Kruskal-Wallis test, p =
701 0.00124; significant p-value in post-hoc tests, $p_{WT\ HL\text{-}WT\ NH}$ = 0.0015). Results for *Df1/+* mice remained
702 unclear due to the low unit counts. For units with only offset responses, the significance for between-
703 group differences was borderline (Kruskal-Wallis test, p = 0.0502).

704 **Supplementary Figure 3**

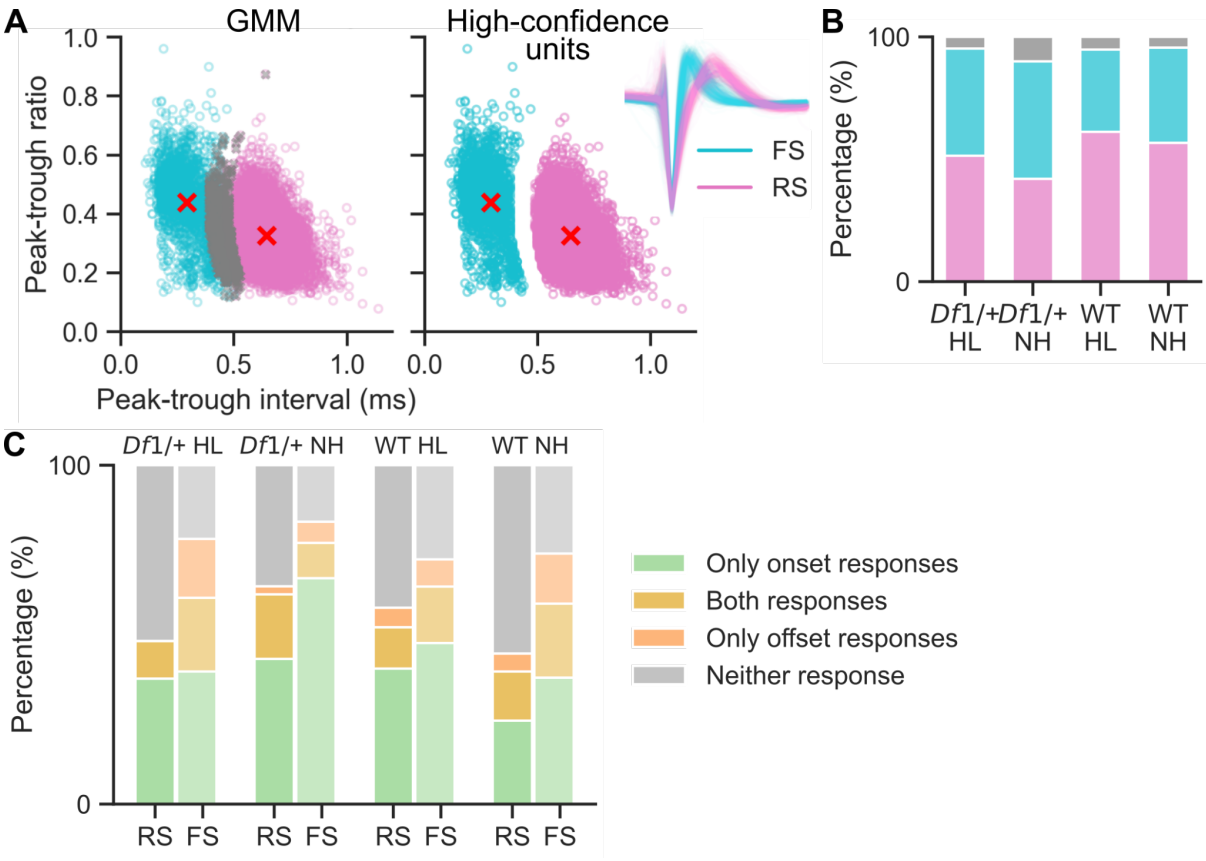

705

706 **Supplementary Figure 3**. **Classification of regular-spiking (RS) and fast-spiking (FS) units and**
707 **their onset and offset response distributions. (A)** After quantifying peak-trough interval and peak-
708 trough ratio of spike waveform in every single unit, a Gaussian mixture model (GMM) was applied to
709 cluster single units into regular-spiking and fast-spiking units. Units within the boundary area were
710 defined as low confidence units and excluded. **(B)** The distribution of RS and FS units in recorded
711 auditory units. **(C)** Fast-spiking units (putative PV+ interneurons) showed higher sensitivities to noise
712 onset and offset transients compared to regular-spiking units (putative excitatory pyramidal neurons).

713 Supplementary Table

714 **Supplementary Table 1**. Hearing profiles in *Df1*/+ mice and WT mice during development. Values
715 indicate mean ± standard error of ABR thresholds (dB SPL) measured in Weeks 4, 6 and 8 for animals
716 in each group.

	Week 4	Week 6	Week 8
Df1/+ HL	Click: 62.35 ± 2.68 8kHz: 73.53 ± 2.53 16kHz: 59.12 ± 1.98 24kHz: 67.65 ± 2.15 32kHz: 83.24 ± 2.61	Click: 59.05 ± 3.04 8kHz: 70.95 ± 3.04 16kHz: 59.05 ± 2.50 24kHz: 68.81 ± 2.71 32kHz: 83.10 ± 2.48	Click: 59.00 ± 2.73 8kHz: 71.50 ± 2.52 16kHz: 59.25 ± 2.06 24kHz: 66.50 ± 2.44 32kHz: 82.25 ± 2.77
Df1/+ NH	Click: 34.50 ± 1.17 8kHz: 51.50 ± 1.98 16kHz: 43.00 ± 1.70 24kHz: 48.00 ± 1.70 32kHz: 61.00 ± 2.33	Click: 36.00 ± 1.00 8kHz: 56.00 ± 5.34 16kHz: 48.00 ± 5.61 24kHz: 57.00 ± 6.24 32kHz: 68.00 ± 4.90	Click: 32.50 ± 1.12 8kHz: 48.33 ± 3.33 16kHz: 39.17 ± 2.01 24kHz: 46.67 ± 3.57 32kHz: 59.17 ± 4.36
WT HL	Click: 56.90 ± 2.57 8kHz: 69.52 ± 2.39 16kHz: 55.95 ± 2.75 24kHz: 66.67 ± 3.19 32kHz: 76.90 ± 3.48	Click: 54.69 ± 2.64 8kHz: 68.12 ± 2.95 16kHz: 54.38 ± 2.37 24kHz: 61.56 ± 3.59 32kHz: 70.00 ± 3.93	Click: 54.00 ± 4.23 8kHz: 71.33 ± 3.98 16kHz: 58.67 ± 3.98 24kHz: 64.67 ± 4.13 32kHz: 78.33 ± 2.66
WT NH	Click: 39.55 ± 2.90 8kHz: 53.18 ± 2.63 16kHz: 49.09 ± 3.08 24kHz: 52.27 ± 2.81 32kHz: 58.64 ± 3.02	Click: 29.17 ± 1.54 8kHz: 50.83 ± 3.00 16kHz: 40.00 ± 3.16 24kHz: 45.00 ± 3.65 32kHz: 52.50 ± 4.61	Click: 35.00 ± 2.24 8kHz: 49.00 ± 4.00 16kHz: 45.00 ± 4.74 24kHz: 55.00 ± 3.16 32kHz: 64.00 ± 3.67

717